Stanford Exploration Project, Report 114, October 14, 2003, pages 45–57

Amplitude balancing of 3-D angle-domain common-image gathers

Biondo Biondi[1]

ABSTRACT

The azimuthal resolution of 3-D Angle Domain Common Image Gathers (ADCIGs) strongly varies with the reflection aperture angle. This dependence may cause severe distortions in the image when 3-D ADCIGs are averaged over azimuths. To correct for these distortions, I derive an effective weighting method based on the jacobian of the transformation to angle domain. The proposed method avoids the underweighting of the reflections close to normal incidence by properly taking into account the "folding" of the azimuth axis. A simple scheme to limit the range of the azimuthal averaging as a function of the opening angle further attenuates noise in the image. A synthetic example illustrates the practical application of the proposed methodology .

INTRODUCTION

Tisserant and Biondi (2003) presented a method to create Angle Domain Common Image Gathers (ADCIGs) in 3-D. In 3-D ADCIGs the image is decomposed at each physical location (x, y, z) depending on the aperture angle γ and the azimuth ϕ of the reflections. Given the the limited azimuthal range of many common acquisition geometries (e.g. marine streamer data), it is often useful to average the ADCIGs over azimuths and to limit the azimuthal average to a subrange of the possible azimuths. These procedures can attenuate coherent noise that was recorded in the data (e.g. multiples) and/or caused by computational shortcuts (Biondi, 2003). However, because of the variable resolution of the angle decomposition in the azimuthal direction, the averaging over azimuths may cause distortions in the amplitudes and the phases of the final image.

In this report I address the problems of 1) balancing the amplitudes across aperture angles while performing the stack over azimuths, 2) determining an "optimal" azimuthal subrange as a function of the aperture angle. Both of these problems are related to the strong dependence of the azimuthal resolution with aperture angle. The azimuthal resolution decreases as the aperture angle gets closer to normal incidence; at the limit, all azimuths are equally illuminated at normal incidence. To preserve the relative amplitudes between the whole range of aperture angles, we need to introduce a proper weighting factor when stacking the ADCIGs over azimuths. If no normalization factor is applied during the summation, the reflections with

[1]**email:** biondo@sep.stanford.edu

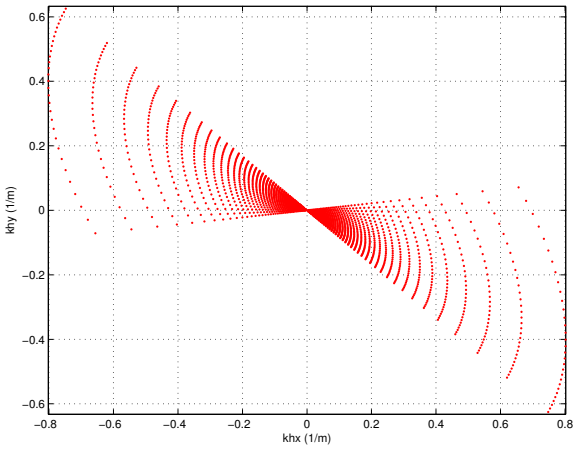

Figure 1: Graphical representation of the mapping from the offset wavenumber $\left(k_{x_h}, k_{y_h}\right)$ plane into the (γ, ϕ) plane. Each dot corresponds to one value of γ and ϕ, for fixed k_z, k_{x_m} and k_{y_m}. biondo1-kh_plane_jac [CR]

angles close to normal incidence would totally overshadow the reflections with wider aperture angles. This normalization factor must be obviously based on the jacobian of the transformation into angle domain, but a straight application of the jacobian would underweight the reflections close to normal incidence. To avoid such a problem, I define a weighting method that takes into account the "wrapping" of the azimuth axis close to normal incidence.

AMPLITUDE CORRECTIONS OF THE MAPPING INTO ANGLE DOMAIN

Tisserant and Biondi (2003) showed that in 3-D the transformation to angle domain is accomplished by mapping the image-domain offset wavenumber plane $\left(k_{x_h}, k_{y_h}\right)$ into the plane defined by the reflection aperture angle γ and the reflection azimuth ϕ. This mapping is performed at fixed depth wavenumber k_z and midpoint wavenumbers k_{x_m} and k_{y_m}.

Appendix A provides the analytical form of this transformation. The analytical form is fairly intricate and not easy to interpret because the reflection azimuth ϕ enters only indirectly as a parameter for rotating the midpoint and offset wavenumbers. Figure 1 shows a graphical representation of the mapping to angle domain, and thus it illustrates the problem that I am addressing in this paper more intuitively than the formulas. The figure shows a uniformly sampled Cartesian grid in the (γ, ϕ) domain mapped into the $\left(k_{x_h}, k_{y_h}\right)$ plane. Each dot corresponds to one value of γ and ϕ, for fixed k_z, k_{x_m} and k_{y_m}. The ranges for γ and ϕ are: $-80^\circ \leq \gamma \leq 80^\circ$ and $-30^\circ \leq \phi \leq 30^\circ$. The dots are densely clustered close to the origin (corresponding to small values of γ), and become sparse away from the origin (corresponding to large values of γ). If this strong variability in the mapping density were not taken into account when a summation is performed in the angle domain, the summation would result in a strongly distorted image.

In this paper I consider the effects of averaging the image over reflection azimuth because it is the most challenging and interesting situation, as we will see briefly. However, similar considerations are needed when summing over aperture angles (for example when computing the "stacked" image after the application of a residual moveout correction to improve reflectors' coherency).

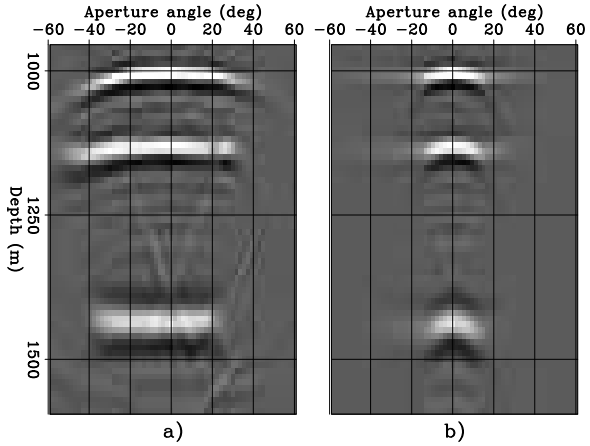

Figure 2: ADCIGs for a synthetic data set. Left: Image for only one azimuth ($\phi = 16°$). Right: Average of ADCIGs for all the azimuth within the range of $-60° \leq \phi \leq 60°$. biondo1-cig-1-data6 [CR]

The effects of ignoring the variability in the mapping density are demonstrated in Figure 2. This figure shows two ADCIGs obtained by imaging a synthetic data set with a full source-receiver 3-D prestack migration. The data set contains 5 dipping planes, from zero dip to 60 degrees dip. The azimuth of the planes is 45 degrees with respect to the direction of the acquisition. The velocity was $V(z) = 1.5 + .5z$ km/s, which corresponds to the upper limit among the typical gradients found in the Gulf of Mexico. The acquisition geometry had one single azimuth and the source-receiver offset range was -1.6–3 km. More detailed description of this data set can be found in (Vaillant and Biondi, 2000; Biondi, 2001, 2003).

Figure 2a shows an ADCIG computed at fixed reflection azimuth ϕ of 16 degrees. This azimuth corresponds – only approximately, because the reflection azimuth changes with the aperture angle – to the reflection azimuth for the deepest reflector. Correspondingly, the deepest reflector has a flat moveout along the aperture angles, but the shallower ones are frowning downward. Figure 2b shows the result of averaging over azimuths all the ADCIGS within the range of $-60° \leq \phi \leq 60°$. In this case the moveouts are flat for all the reflection angles larger than 10 degrees, but the amplitude of the image is strongly attenuated for all these angles. This distortion of the image amplitudes is caused by the variable density of the mapping from the the $\left(k_{x_h}, k_{y_h}\right)$ plane into the (γ, ϕ) plane illustrated in Figure 1.

The solution to this problem seems straightforward. We can correct the amplitudes by applying the jacobian of the transformation from the $\left(k_{x_h}, k_{y_h}\right)$ plane into the (γ, ϕ) plane (Appendix A presents the formulas to evaluate the jacobian). However, while this correction yields a much improved result, it is not sufficient. Figure 3a shows the effect of including the jacobian while transforming the image into angle domain. The amplitudes of the ADCIG are now distorted in the opposite direction of the previous result (Figure 2b). Now the wide aperture angles have a good amplitude response, but the narrow angles have been too strongly attenuated and the $\gamma = 0$ trace has been zeroed. This behavior is simply explained by the fact that the jacobian is zero at $\gamma = 0$. This singularity of the jacobian is graphically represented in Figure 1 by the fact that all the dots corresponding to $\gamma = 0$ fall into the origin of the plane, where the dot density becomes effectively infinite.

A simple solution to this problem is suggested when we examine the inverse mapping, as it is graphically illustrated in the sketch in Figure 4. In this case an integration segment

along the line defined by constant γ and close to the origin of the $\left(k_{x_h}, k_{y_h}\right)$ plane would expand into a long segment extending well beyond the usual range of $-180^\circ \leq \phi \leq 180^\circ$. However, because of the periodicity of the mapping, the segment is actually folded into the the $-180^\circ \leq \phi \leq 180^\circ$, and its effective length is limited to 360 degrees (2π). Taking into account of this fact, we can correct the jacobian weighting and recover the image amplitudes close to normal incidence. The details of the correction and its derivation are presented in Appendix A.

The effects of taking into account the folding of the azimuth axis in the mapping are demonstrated in Figure 3b. Now the angles close to near incidence have been properly imaged. Figure 5 shows windows of the ADCIGs shown in Figure 3 with narrower aperture angle ranges. The comparison of Figure 5a and Figure 5b demonstrates the improvements achieved by taking into account the folding of the azimuth axis.

Figures 6–7 illustrate the effect of the amplitude correction from another point of view. They show depth slices taken at the depth of 1,140 meters (corresponding to the reflector dipping at 45 degrees) before the stacking over azimuths. The reflection amplitudes are thus shown as function of both the aperture angle γ and the azimuth ϕ. Because of the poor azimuthal resolution close to normal incidence, the azimuthal range is wide for small γ; it narrows as γ increases. Comparing Figure 6 with Figure 7 it is evident that the amplitude correction boost up the relative amplitudes of the image at large γ.

Relative phase shift across aperture angles (γ)

A close examination of both Figure 3 and Figure 5 reveals that the smaller aperture angles ($\gamma \leq 8$) have a slight phase shift with respect to the rest of the aperture angles. A "frowning" artifact that is related to this phase shift is also visible in the gathers. This artifact is attenuated by limiting the azimuthal range of the summation, as described in the next section. Comparison of Figures 3–5 with Figure 2a also suggests that the phase shift is caused by the stacking over azimuths, since it is absent in the gather shown in Figure 2a.

The phase shift is indeed related to the summation over azimuth and it is easily explained by the analysis of the image as a function of the reflection azimuth ϕ and at constant aperture angle γ. The three panels in Figure 8 show such sections for three different aperture angles: a) $\gamma = 4^\circ$, b) $\gamma = 20^\circ$, and c) $\gamma = 35^\circ$. The curvature of the reflectors as a function of the azimuth is different in Figure 8a from both Figure 8b and Figure 8c. These differences in the curvature of the reflector cause the relative phase shift of the stacked gathers shown in Figures 3–5. In other words, the phase shift at large aperture angles ($\gamma > 8$) is caused by the interference of the flanks of the hyperbolic curves shown in Figures 3–5 with the correct summation of the flat spots of the same hyperbolic curves.

Fortunately, both the phase shift and the "frowning" artifact are related to the illumination of the reflectors by the data (common-azimuth acquisition geometry) and they are not caused by the methodology employed to image the data. As the azimuthal range of the data increases, the flat spots at the top of the hyperbolic curves shown in Figures 3–5 should widen. Consequently, when stacking over azimuths the influence of the flanks should decrease relative to

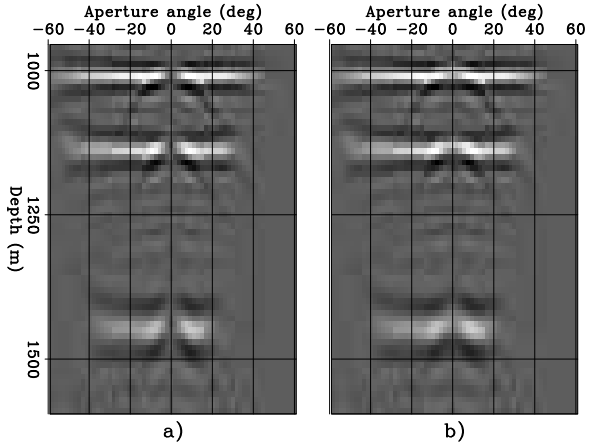

Figure 3: ADCIGs for a synthetic data set. Left: Image obtained when the simple jacobian weighting is applied before averaging over azimuths. Right: Image obtained when the jacobian weighting takes into account the folding of the azimuth axis. biondo1-cig-2-data6 [CR]

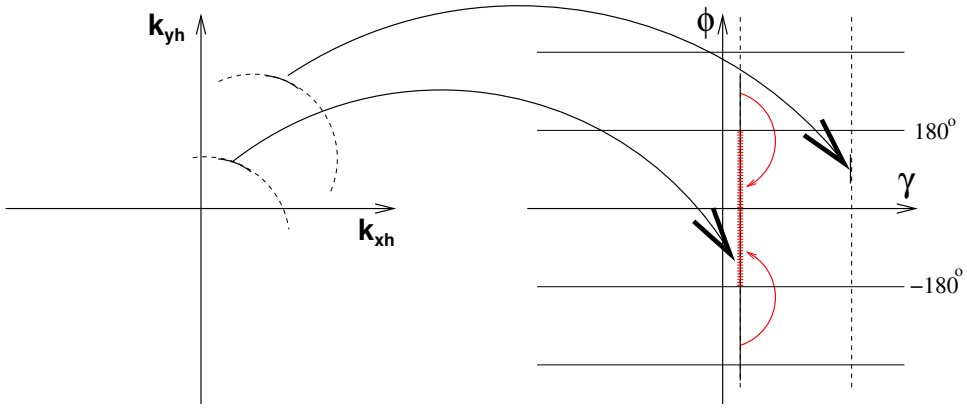

Figure 4: Graphical representation of the stretching involved in the mapping from the (k_{x_h}, k_{y_h}) plane into the (γ, ϕ) plane. biondo1-fold [NR]

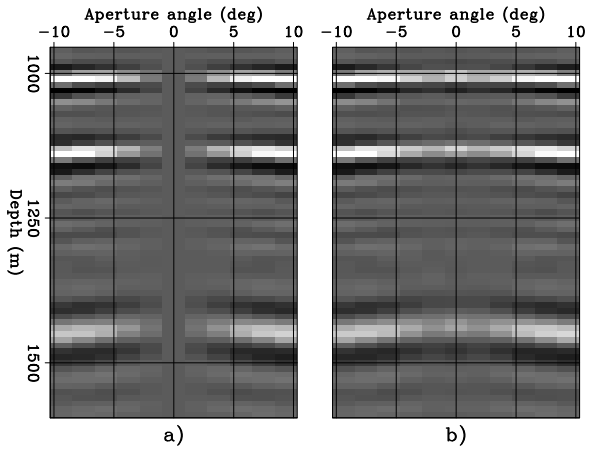

Figure 5: Zoom into the ADCIGS shown in Figure 3 to examine the differences between the two panels close to normal incidence. biondo1-cig-2-data6-win [CR]

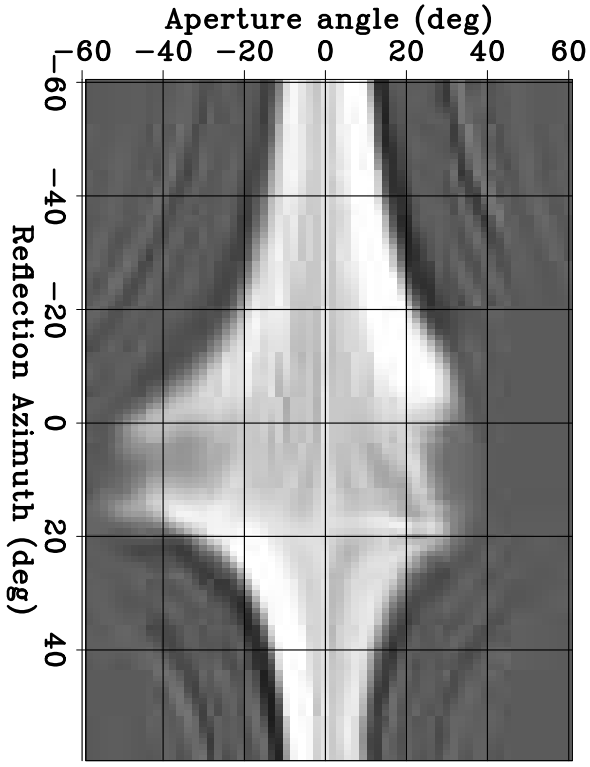

Figure 6: Depth slice taken at the depth of 1,140 meters (corresponding to the reflector dipping at 45 degrees) before the stacking over azimuths. Notice that the azimuthal resolution is strongly dependent on the aperture angle. biondo1-zaz-60-60-dense-all-v3-data6 [CR]

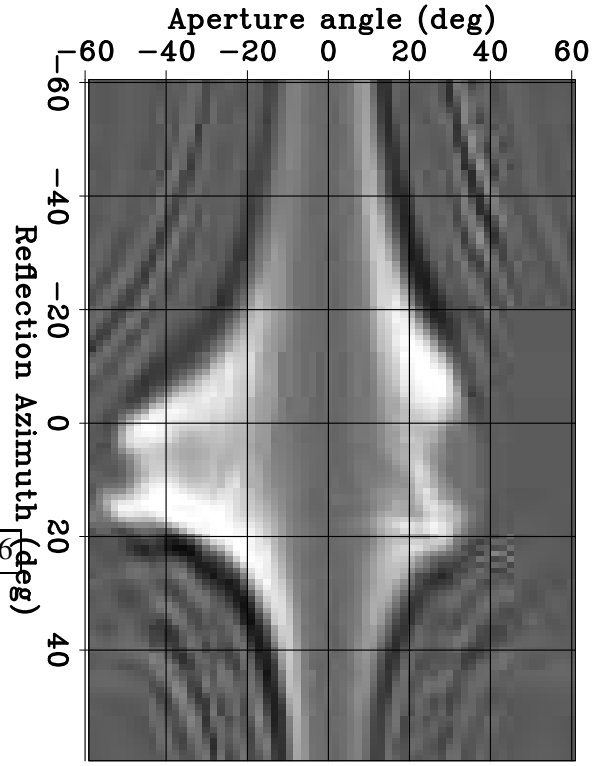

Figure 7: Depth slice taken at the same depth as the slice shown in Figure 6 (z=1,1140 meters) after application of the proposed angular dependent weighting. Notice that the amplitudes close to normal incidence have been attenuated, but not zeroed, and the ones at large aperture angle have been boosted up. biondo1-zaz-60-60-dense-all-jac-v3-data6 [CR]

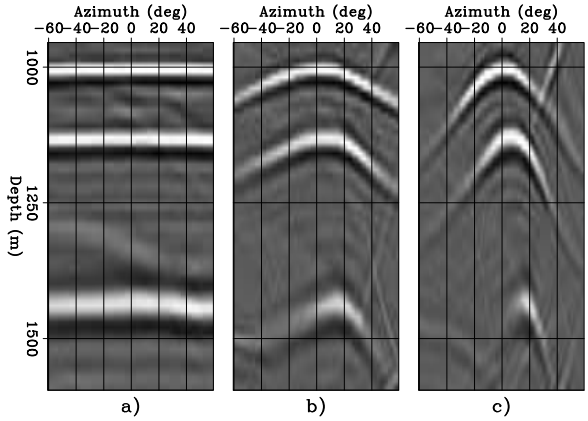

Figure 8: Image as function of the reflection azimuth at constant aperture angle: a) $\gamma = 4°$, b) $\gamma = 20°$, and c) $\gamma = 35°$. biondo1-azim-gamma-all [CR]

the influence of the flat spot, and the phase shift should disappear. It would be interesting to confirm this hypothesis with a real data example from a marine data set.

Determining the azimuthal range

It is often useful to limit the azimuthal range of the image. Given the strong dependence of the azimuthal resolution with aperture angle, it is natural to make the bounds of the azimuthal range functions of the aperture angle γ. Any smooth function of γ is probably adequate to define the azimuthal boundaries. I decided to apply a trigonometric function to transition between the limits at normal incidence and the limits at 90 degrees. If $\gamma_{\max}$ is the maximum aperture angle, $\phi^0_{\min}$ and $\phi^0_{\max}$ are respectively the minimum and maximum azimuth angles for $\gamma = 0$ degrees, and $\phi^{90}_{\min}$ and $\phi^{90}_{\max}$ are respectively the minimum and maximum azimuth angles for $\gamma = 90$ degrees, then I set the azimuthal limits $\phi^{\gamma}_{\min}$, $\phi^{\gamma}_{\max}$, by applying the following expressions:

$$\phi^{\gamma}_{\min} = \phi^{90}_{\min} + \left(\phi^0_{\min} - \phi^{90}_{\min}\right)\left[\sin\left(\frac{90-\gamma}{90}\right)\right]^p, \tag{1}$$

$$\phi^{\gamma}_{\max} = \phi^{90}_{\max} + \left(\phi^0_{\max} - \phi^{90}_{\max}\right)\left[\sin\left(\frac{90-\gamma}{90}\right)\right]^p, \tag{2}$$

where p is a free parameter that determines the shape of the azimuthal window.

Figure 9 is a generalization of Figure 1. The red (darker in gray scale) dots are the same as in Figure 1, and represent the mapping into angle domain with $\phi^0_{\min} = \phi^{90}_{\min} = -30$ degrees, and $\phi^0_{\max} = \phi^{90}_{\max} = 30$ degrees. The green (lighter in gray scale) is the mapping when the azimuthal range is broader close to normal incidence, that is with $\phi^0_{\min} = -90$ degrees, and $\phi^0_{\max} = 90$ degrees, and $p = 3$. Notice that the integration domain represented by the green dots (lighter in gray scale) does not shrink close to the origin, as the original integration domain does.

Figure 10 shows the effect of the variable azimuthal range on the synthetic data set. Figure 10b shows the same ADCIG as in Figure 3b. The azimuthal range was constant over γ; that is $\phi^0_{\min} = \phi^{90}_{\min} = -60$ degrees, and $\phi^0_{\max} = \phi^{90}_{\max} = 60$ degrees. Figure 10a shows the ADCIG extracted at the same location as the one in Figure 10b, but obtained with variable

azimuthal range. The parameters were $\phi^0_{\text{min}} = -60$ degrees, $\phi^{90}_{\text{min}} = -5$ degrees, $\phi^{90}_{\text{max}} = 25$ degrees, $\phi^0_{\text{max}} = 60$ degrees, and $p = 3$. The reduction in the azimuthal range attenuates the numerical noise in the image. In particular, it attenuates the "frowning" artifacts that, as I discussed in the previous section, are related to the narrow azimuthal coverage of the data.

Figure 11 shows a depth slice extracted from the image at the same depth as the slices shown in Figures 6–7, but with the variable azimuthal range defined by the parameters listed above. The comparison of Figure 11 with Figure 7 demonstrates that the window defined using the relationships (1) and (2) preserves the coherent energy of the event, while removing noise.

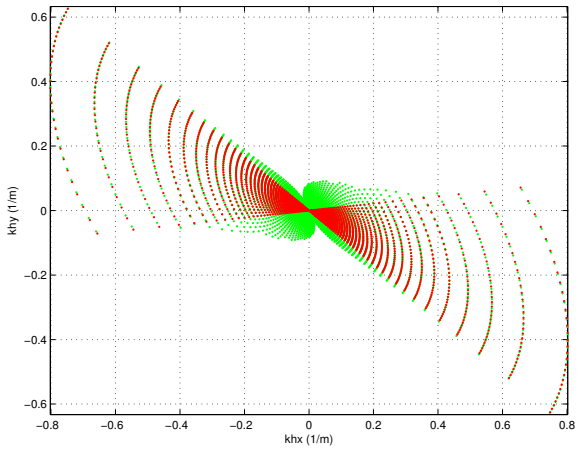

Figure 9: Graphical representation of the effects of the variable azimuthal range on the mapping from the offset wavenumber (k_{x_h}, k_{y_h}) plane into the (γ, ϕ) plane. The green (lighter in gray scale) dots correspond to the mapping with variable azimuthal range. biondo1-kh_plane_wide [CR]

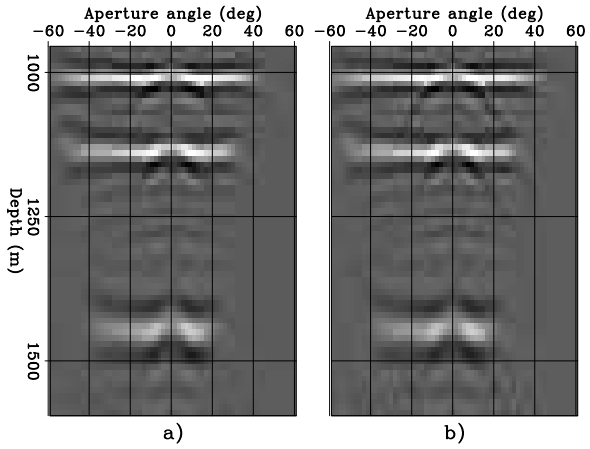

Figure 10: ADCIGs for a synthetic data set. Left: Image obtained after application of both the angular dependent weighting and the variable azimuthal range. Right: Image obtained after application of the angular dependent weighting. biondo1-cig-3-data6 [CR]

CONCLUSIONS

To avoid distortion in the image, 3-D ADCIGs must be properly weighted before averaging over azimuths. These weights can be derived from the jacobian of the transformation to angle domain, after taking into account the folding of the azimuth axis. The weighting method I presented was successful to correct the image obtained from a synthetic data set.

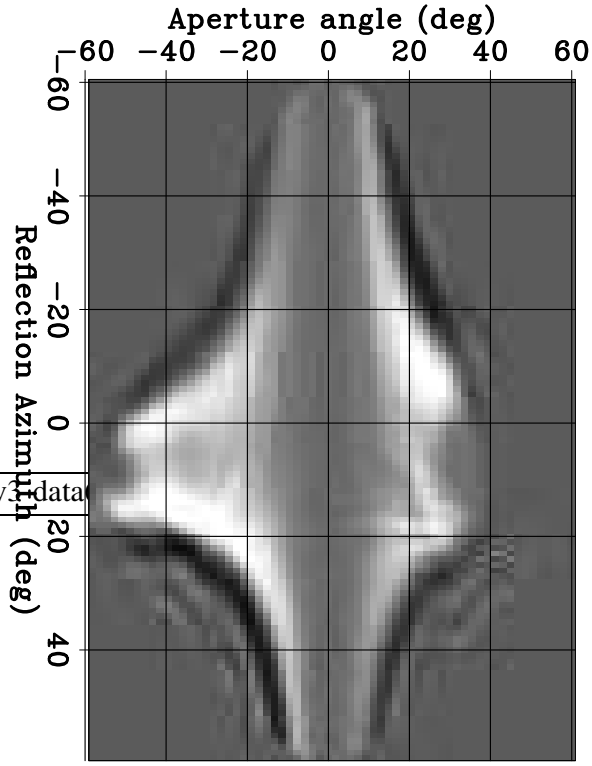

Figure 11: Depth slice taken at the same depth as the slice shown in Figure 7 (z=1,1140 meters), after application of both the angular dependent weighting and the variable azimuthal range. biondo1-zaz-60-60-dense-all-jac-bound-v3 [CR]

To attenuate both coherent noise and numerical artifacts, I also defined a simple scheme for limiting the azimuthal range of the image. This variable azimuthal range proved to be useful in reducing the artifacts caused by the limited azimuthal coverage of the synthetic data. Further analysis of the artifacts caused by the azimuthal coverage of real acquisition geometries might be required to make the computation of 3-D ADCIGs a robust tool for velocity analysis and amplitude analysis.

REFERENCES

Biondi, B., 2001, Narrow-azimuth migration: Analysis and tests in vertically layered media: SEP–**108**, 105–118.

Biondi, B., 2003, Narrow-azimuth migration of marine streamer data: SEP–**113**, 107–120.

Tisserant, T., and Biondi, B., 2003, Wavefield-continuation angle-domain common-image gathers in 3-D: SEP–**113**, 211–220.

Vaillant, L., and Biondi, B., 2000, Accuracy of common-azimuth migration approximations: SEP–**103**, 157–168.

APPENDIX A

This appendix derives the expressions for the weights to be applied to the ADCIGs before averaging over azimuths. These weights are based on the jacobian of the transformation into angle domain. The first step is therefore to find the expressions for evaluating this jacobian.

The starting point for computing the jacobian is the transformation into angle domain. Tisserant and Biondi (2003) showed that 3-D ADCIGs can be computed according to the following mappings:

$$k'_{x_h} = -\tan\gamma\sqrt{k'^2_{y_m}+k_z^2}, \tag{A-1}$$

$$k'_{y_h} = -\frac{k'_{y_m}k'_{x_m}k'_{x_h}}{k_z^2+k'^2_{y_m}}; \tag{A-2}$$

$$\tag{A-3}$$

where the primes on the wavenumber indicate the rotation of the coordinate axis by ϕ according to the following relationships:

$$k'_{x_m} = \cos\phi k_{x_m} - \sin\phi k_{y_m}, \tag{A-4}$$

$$k'_{y_m} = \sin\phi k_{x_m} + \cos\phi k_{y_m}, \tag{A-5}$$

and similarly

$$k'_{x_h} = \cos\phi k_{x_h} - \sin\phi k_{y_h}, \tag{A-6}$$

$$k'_{y_h} = \sin\phi k_{x_h} + \cos\phi k_{y_h}. \tag{A-7}$$

We need to compute the partial derivatives of the offset wavenumbers at constant aperture angle γ. Therefore, we start from rewriting the coplanarity condition in equation (A-2) in terms of reflections angles in the rotated coordinate system: the aperture angle γ', the in-line dip angle α'_x, and the cross-line dip angle α'_y. The following relationships link the wavenumber in the image domain to these angles

$$\tan\alpha'_x = \frac{k'_{x_m}}{k_z}, \tag{A-8}$$

$$\tan\alpha'_y = \frac{k'_{y_m}}{k_z}, \tag{A-9}$$

and

$$\tan\gamma' = -\cos\alpha'_y\frac{k'_{x_h}}{k_z}. \tag{A-10}$$

Then equation (A-2) becomes:

$$k'_{y_h} = k_z\tan\gamma'\tan\alpha'_x\sin\alpha'_y, \tag{A-11}$$

and equation (A-1) becomes:

$$k'_{x_h} = -k_z\frac{\tan\gamma'}{\cos\alpha'_y}. \tag{A-12}$$

Evaluation of $\partial k'_{x_h}/\partial\phi$ and $\partial k'_{y_h}/\partial\phi$

Differentiating equation (A-12) and after some algebraic manipulation, we obtain the following:

$$\begin{aligned}\frac{\partial k'_{x_h}}{\partial\phi} &= -k_z\tan\gamma\frac{\partial\left(\frac{1}{\cos\alpha'_y}\right)}{\partial\phi}\\ &= -k_z\tan\gamma\frac{\partial\left(\frac{1}{\cos\alpha'_y}\right)}{\partial k'_{y_m}}\frac{\partial k'_{y_m}}{\partial\phi}\\ &= -k_z\tan\gamma\frac{\sin\alpha'_y}{k_z}\frac{\partial k'_{y_m}}{\partial\phi}\\ &= -\tan\gamma\sin\alpha'_y\frac{\partial k'_{y_m}}{\partial\phi}.\end{aligned} \tag{A-13}$$

Differentiating equation (A-11) we can write the following:

$$\frac{\partial k'_{y_h}}{\partial\phi} = k_z\tan\gamma\left[\frac{\partial\tan\alpha'_x}{\partial\phi}\sin\alpha'_y + \frac{\partial\sin\alpha'_y}{\partial\phi}\tan\alpha'_x\right]. \tag{A-14}$$

To evaluate equation (A-14) we need $\partial\tan\alpha'_x/\partial\phi$ and $\partial\sin\alpha'_y/\partial\phi$; that is,

$$\frac{\partial\tan\alpha'_x}{\partial\phi} = \frac{\partial\tan\alpha'_x}{\partial k'_{x_m}}\frac{\partial k'_{x_m}}{\partial\phi} = \frac{1}{k_z}\frac{\partial k'_{x_m}}{\partial\phi}, \tag{A-15}$$

and

$$\frac{\partial\sin\alpha'_y}{\partial\phi} = \frac{\partial\sin\alpha'_y}{\partial k'_{y_m}}\frac{\partial k'_{y_m}}{\partial\phi} = \frac{1}{k_z}\cos^3\alpha'_y\frac{\partial k'_{y_m}}{\partial\phi}. \tag{A-16}$$

Substituting equation (A-15) and equation (A-16) into equation (A-14), we finally obtain:

$$\begin{aligned}\frac{\partial k'_{y_h}}{\partial\phi} &= k_z\tan\gamma\left[\frac{\sin\alpha'_y}{k_z}\frac{\partial k'_{x_m}}{\partial\phi} + \frac{\tan\alpha'_x}{k_z}\cos^3\alpha'_y\frac{\partial k'_{y_m}}{\partial\phi}\right]\\ &= \tan\gamma\left[\sin\alpha'_y\frac{\partial k'_{x_m}}{\partial\phi} + \tan\alpha'_x\cos^3\alpha'_y\frac{\partial k'_{y_m}}{\partial\phi}\right].\end{aligned} \tag{A-17}$$

Evaluation of $\partial k_{x_h}/\partial\phi$ and $\partial k_{y_h}/\partial\phi$

Equations (A-13) and (A-17) express the partial derivatives of the offset wavenumbers in the rotated coordinates. We need to evaluate the partial derivatives of the offset wavenumbers in the data coordinates. Therefore, we need to differentiate the expressions defining the inverse rotation; that is, differentiate with respect to ϕ the following expressions:

$$k_{x_h} = \cos\phi k'_{x_h} + \sin\phi k'_{y_h}, \tag{A-18}$$

$$k_{y_h} = -\sin\phi k'_{x_h} + \cos\phi k'_{y_h}. \tag{A-19}$$

The partial derivatives are then given by the following expressions:

$$\frac{\partial k_{x_h}}{\partial \phi} = \cos\phi \frac{\partial k'_{x_h}}{\partial \phi} + \sin\phi \frac{\partial k'_{y_h}}{\partial \phi} - \sin\phi k'_{x_h} + \cos\phi k'_{y_h}, \tag{A-20}$$

$$\frac{\partial k_{y_h}}{\partial \phi} = -\sin\phi \frac{\partial k'_{x_h}}{\partial \phi} + \cos\phi \frac{\partial k'_{y_h}}{\partial \phi} - \cos\phi k'_{x_h}. - \sin\phi k'_{y_h}. \tag{A-21}$$

Computation of scaling factor $W_{\gamma,\phi}$

The last step is the computation of the scaling factor $W_{\gamma,\phi}$ from the partial derivatives $\partial k_{x_h}/\partial\phi$ and $\partial k_{y_h}/\partial\phi$.

The unit vector $\mathbf{u}$ tangent to the integration line at constant γ is given by

$$\mathbf{u} = \left(\frac{\frac{\partial k_{x_h}}{\partial \phi}}{\sqrt{\frac{\partial k_{x_h}}{\partial \phi}^2 + \frac{\partial k_{y_h}}{\partial \phi}^2}} \mathbf{x} + \frac{\frac{\partial k_{y_h}}{\partial \phi}}{\sqrt{\frac{\partial k_{x_h}}{\partial \phi}^2 + \frac{\partial k_{y_h}}{\partial \phi}^2}} \mathbf{y} \right). \tag{A-22}$$

The mapping along the azimuth axis of a vector of the same direction as $\mathbf{u}$ and length proportional to the sampling in the offset wavenumber domain $\left(\Delta k_{x_h}, \Delta k_{y_h}\right)$ is a segment of length

$$\delta\phi = \frac{2\sqrt{\Delta k_{x_h}^2 + \Delta k_{y_h}^2}}{\sqrt{\frac{\partial k_{x_h}}{\partial \phi}^2 + \frac{\partial k_{y_h}}{\partial \phi}^2}}. \tag{A-23}$$

If $\Delta\phi$ is the azimuthal range of the stacking at $\gamma = 0$, the scaling factor is set as in the following:

$$W_{\gamma,\phi} = \begin{cases} 1 & \text{if } \delta\phi \geq \Delta\phi \\ \\ \frac{\Delta\phi}{\delta\phi} & \text{if } \delta\phi < \Delta\phi. \end{cases} \tag{A-24}$$